Simultaneous Pulse Combination and Nearly Self-Similar Pulse Compression in Tapered Silicon Waveguides at Around 2.0 μm

Jiayao Huang, *Student Member, IEEE*, Feng Ye, *Student Member, IEEE*, and Qian Li, *Senior Member, IEEE*

***Abstract*—Nonlinear pulse compression technology permits practitioners to produce ultrashort pulses for integrated frequency comb generation and optical coherence tomography. However, on-chip simultaneous combination and compression of two pulses at 2.0 μm is a complex nonlinear dynamic that has never been reported. Here, we demonstrate that two raised cosine pulses with the same center wavelengths of 2.0 μm are firstly coalesced into a single combined pulse and then realize nearly self-similar compression in the dispersion exponentially decreasing silicon waveguide, where the final compressed pulse was reduced from 200 fs to 49 fs with a compression factor of 4.08. Additionally, the peak power of the compressed pulse steadily rises to 2.16 times of the initial peak power. For further development, we also illustrate two input pulses with different center wavelengths to realize effective combination and self-similar compression. These results shed new insights into the potential of dispersion engineering waveguides for low-power integrated applications at 2.0 μm.**

***Index Terms*—Self-similar pulse compression, silicon-based waveguide, mid-infrared, nonlinear optics.**

I. Introduction

WHILE the ultrashort pulses naturally appears in 2-μm waveband, the potential applications at this wavelength have attracted notable interest in eye safety [1], biomedical engineering [2], atmospheric security [3], and frequency combs generation [4]. Recently, the advanced gain materials enable numerous mid-IR fiber laser systems to generate mid-IR ultrashort pulses, which provides the superiorities of compact, high-efficiency and good beam quality [5]. 2.0 μm fiber lasers provide an unparalleled advantage to significantly enhance the mid-/far-infrared (IR) wavelength conversion efficiency without notable two-photon absorption (TPA) [6], which is beneficial to achieve the spectral absorption molecular fingerprint region that can identify plentiful information about the molecular composition, structure and conformation [7], [8]. Up to date, integrated photonic devices demonstrate excellent superiorities in these applications, including high compatibility with CMOS fabrication facilities, large-scale photonic integrated circuits and favorable high power/energy efficiency [9]. Recently, CMOS-chip based pulse compression technologies have been widely reported from communication band to mid-infrared band, which consists of high-order pulse compression [10]–[12], Bragg soliton compression [13], adiabatic pulse compression [14], cascaded pulse compression [15], [16] and self-similar pulse compression [17]–[21]. Particularly, pulse compression schemes have also been explored in multiple material platforms such as silicon [11], chalcogenide-silicon [19], silicon nitride [22], ultra-silicon-rich nitride [13] and so on. In parallel, progress in the chip-based self-similar pulse compression has allowed access to attain the integrally chirp-free and pedestal-free femtosecond pulse, which possesses the advantages of nearly transform-limited characteristic and avoiding pulse breakup even at high peak powers [17]–[19]. In this process, the nonlinearity is desired to produce new frequencies by the self-phase modulation (SPM), while the anomalous group-velocity dispersion (GVD) is necessary for decreasing exponentially to maintain the balance of the soliton evolution [23].

Previously, much of the advances on pulse compression has concentrated on the single-pulse compression. To obtain the extra functionalities of pulse controlling, the efficient multiple-pulses combination and compression was firstly proposed in the exponentially dispersion decreasing nonlinear fiber, which indicates the ultimate compressed pulse possesses higher energy and comprises major portion of the total input light wave energy [24], [25]. However, the optical fiber is placing a serious challenge on the miniaturization and integration in the chip-scale. Compared with the kilometer-long fibers, silicon photonics has emerged as the progressive technology to provides large nonlinearity, extensive transparency range and accurate dispersion engineering for pulse compression in the centimeter-long waveguides [18]. Owing to the acceptable TPA and low absorption loss [26], [27], silicon platform is a good choice to achieve pulses combination and compression at 2.0 μm. From previous literature, most pulse compression methods obtain output pulse by directly compressing a single input pulse. To the best of our knowledge, it is the first time to demonstrate the two pulses combination and compression in the tapered silicon waveguide, which is a new pulse compression scheme to produce high-power ultrashort

Manuscript received March 10, 2022; revised June 1, 2022; accepted June 3, 2022. Date of publication June 10, 2022; date of current version June 21, 2022. This work was supported in part by Shenzhen Science and Technology Innovation Commission under Grant GXWD20201231165807007-20200827130534001, and in part by the Youth Science and Technology Innovation Talent of Guangdong Province under Grant 2019TQ05X227. *(Corresponding author: Qian Li.)*

The authors are with the School of Electronic and Computer Engineering, Peking University, Shenzhen 518055, China (e-mail: huangjiayao@pku.edu.cn; ye-feng@pku.edu.cn; liqian@pkusz.edu.cn).

Digital Object Identifier 10.1109/JPHOT.2022.3181288

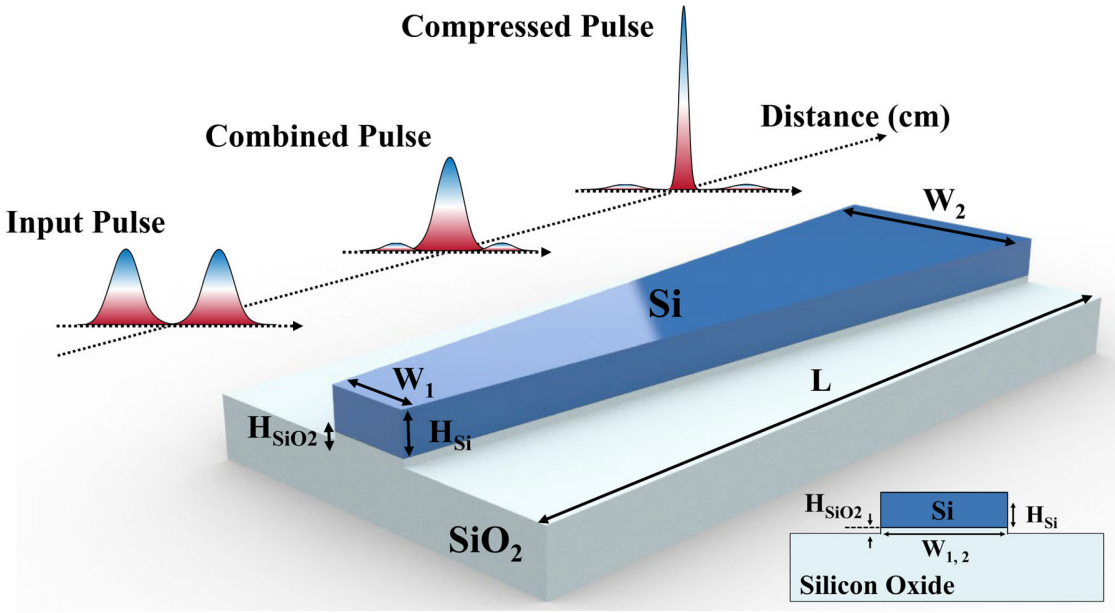

Fig. 1. 3D conceptual design of the integrated Si-TPCC device with the parameters represented as: waveguide width of the input and output segment (W_1 and W_2), silicon core height (H_{Si}), silica layer height ($H_{\mathrm{SiO_2}}$) and optimal waveguide length (L). The inset figure is the cross-section of the silicon waveguide which is surrounding by air-cladding and buried oxide substrate. The diagram of temporal evolution is demonstrated in the figure, where the input pulses are preliminarily combined into a single pulse and a nearly self-similar pulse compression can be further implemented in the tapered silicon waveguide.

pulse from different wavelength laser sources in the chip-scale devices.

In this article, we investigate the two pulses combination and compression in the silicon waveguide (Si-TPCC) theoretically and numerically, which is a creative method to control the ability of the pulse compression performance in the integrated devices. To initiate the Si-TPCC process, we employ two raised cosine (RC) pulses which share the same initial chirp. As shown in Fig. 1(a), those chirped pulses are transmitted into the silicon waveguide with the exponentially decreasing dispersion, where they coalesce into a single pulse in primary and further experiences nearly self-similar pulse compression.

II. Theoretical Models

For a further investigation, simulations of the Si-TPCC processes were performed as generalized nonlinear Schrödinger equation (GNLSE) and modified by TPA, free-carrier effects and stimulated Raman scattering for a tapered silicon waveguide [28], [29],

$$\frac{\partial A\left(z,t\right)}{\partial z}=\sum_{k\geq 2}i^{k+1}\frac{\beta_k(z)}{k!}\frac{\partial^k A}{\partial t^k}-\frac{\alpha_{\mathrm{c}}}{2}\left(1+i\mu\right)A-\frac{\alpha_0}{2}A+i\gamma_e\left(1+\frac{i}{\omega_0}\frac{\partial}{\partial t}\right)\times\left(A\int_0^{\infty}R\left(t-t'\right)\left|A\left(z,t'\right)\right|^2dt'\right),\tag{1}$$

where $A(z,t)$ is the pulse envelope of the electric field and $\alpha_0=0.2\,\mathrm{dB/cm}$ is the linear loss in the waveguide [4]. Further, $\beta_k(z)$(m = 1, 2, …, and *k*) represents the *k*-th order dispersion and the influence of all higher-order dispersion is considered for pulse compression, where the infinite dispersion in Eq. (1) can be rewritten in the frequency domain [30],

$$\mathcal{F}\left[\sum_{k=2}^{\infty}i\frac{i^k\beta_k}{k!}\frac{\partial^k A}{\partial t^k}\right]=i[\beta\left(\omega\right)-\beta\left(\omega_0\right)-\beta_1\left(\omega_0\right)\left(\omega-\omega_0\right)]\widetilde{A}\left(\omega\right)\tag{2}$$

where $\beta(\omega)=n_{\mathrm{eff}}(\omega)\omega/c$, $\beta_1(\omega)=\partial\beta/\partial\omega$, and $\mathcal{F}$ is the Fourier transform operator. $\gamma_e=\gamma+i\alpha_{\mathrm{TPA}}$ is the complex nonlinear coefficient, which is determined by both nonlinear coefficient (γ) and TPA loss coefficient (α_{TPA}). In addition, ω_0 is the center frequency of the input pulse, which responses to the initial center wavelength of $\lambda_0=2000\,\mathrm{nm}$. The free carrier absorption loss is defined as $\alpha_{\mathrm{c}}=\sigma_{\mathrm{c}}N_{\mathrm{c}}$, where N_{c} is the free carrier density and $\sigma_{\mathrm{c}}=2.41\times10^{-21}\mathrm{m}^2$ is the free carrier absorption coefficient for silicon [31]. The parameter $\mu=3.06$ accounts for the free carrier dispersion [28]. In practice, the free carrier density N_{c} in the waveguide takes the form [29], [32],

$$\frac{\partial N_{\mathrm{c}}\left(z,t\right)}{\partial t}=\frac{\beta_{\mathrm{TPA}}}{2h\nu_0}\frac{\left|A\left(z,t\right)\right|^4}{A_{\mathrm{eff}}^2}-\frac{N_{\mathrm{c}}}{\tau_{\mathrm{eff}}},\tag{3}$$

$$A_{\mathrm{eff}}=\frac{\left(\int\int_{-\infty}^{+\infty}\left|F\left(x,y\right)\right|^2dxdy\right)^2}{\int\int_{-\infty}^{+\infty}\left|F\left(x,y\right)\right|^4dxdy}\tag{4}$$

$$\gamma=\frac{2\pi n_2}{\lambda A_{\mathrm{eff}}}+i\frac{\beta_{\mathrm{TPA}}}{2A_{\mathrm{eff}}}\tag{5}$$

where $h\nu_0$ is the photon energy and $\tau_{\mathrm{eff}}=3\mathrm{ns}$ is the free carrier lifetime [29]. $n_2=1.1\times10^{-17}\mathrm{m}^2/\mathrm{W}$, $\beta_{\mathrm{TPA}}=2.5\times10^{-12}\mathrm{m/W}$ and A_{eff} account for the nonlinear refractive index, TPA coefficient and the effective mode area [31], [33]. The

nonlinear response function in waveguide is denoted by [32],

$$R(t) = (1 - f_{\mathrm{R}})\,\delta(t) + f_{\mathrm{R}} h_{\mathrm{R}}(t), \tag{6}$$

where $f_{\mathrm{R}} = 0.043$ is the fractional contribution of the delayed Raman, and $h_{\mathrm{R}}(t)$ is the Raman response function,

$$h_{\mathrm{R}}(t) = \frac{\tau_1^2 + \tau_2^2}{\tau_1 \tau_2^2} \exp\left(-\frac{t}{\tau_2}\right) \sin\left(\frac{t}{\tau_1}\right), \tag{7}$$

where $\tau_1 = 10\,\mathrm{fs}$ and $\tau_2 = 3\,\mathrm{ps}$.

From the analysis in the previous research, the realization of the Si-TPCC process depends strongly upon the GVD decreasing exponentially [24], [25]. In this line, the decreasing exponentially GVD is described approximately as,

$$\beta_2(z) = \beta_{20} \exp(-\sigma z), \sigma = \alpha_{20}\beta_{20} \tag{8}$$

where, β_{20}, α_{20} and σ are the initial dispersion value, initial chirp coefficient and second-order dispersion decay rate [18].

To ensure broader applicability of the same or different central wavelengths, we employ the following two chirped RC pulses to examine the Si-TPCC, which are expressed as [25],

$$\frac{\sqrt{P_0}}{2}\left\{1+\cos\left[\pi\left(t/T_0+1\right)\right]\right\} \exp\left(i\alpha_{20}t^2/2\right), t/T_0 \in [-2, 0], \tag{9}$$

$$\frac{\sqrt{P_0}}{2}\left\{1+\cos\left[\pi\left(t/T_0+1\right)\right]\right\} \exp\left(i2\pi\Delta\nu t\right) \exp\left(i\alpha_{20}t^2/2\right), t/T_0 \in [0, 2], \tag{10}$$

where T_0, P_0 and $\Delta\nu$ are the sign of the initial pulse width, initial peak power ($P_0 = 0.5|\beta_{20}|/\gamma/T_0^2$) and the variation between the center frequencies of the two input pulses.

III. Investigation on Mid-Infrared Pulses Combination and Compression in Silicon Tapered Waveguide

A. Modeling a Tapered Silicon Waveguide

The schematic diagram of the 3D view and a cross section view of the proposed structure are illustrated in Fig. 1, which consists of a tapered silicon waveguide and a silica substrate. Our designed device provides a vast flexibility for dispersion engineering, where the geometric parameters are fully optimized and selected as $H_{\mathrm{Si}} = 390\,\mathrm{nm}$, $H_{\mathrm{SiO_2}} = 10\,\mathrm{nm}$, $L = 4\,\mathrm{cm}$, $W_1 = 580\,\mathrm{nm}$ and $W_2 = 1300\,\mathrm{nm}$. Note that the silicon waveguide is etched excessively into the silica substrate for 10 nm to reduce the linear loss and the similar waveguide has been fabricated to generate mid-infrared frequency comb in a CMOS pilot line [21]. Fig. 2(a) denotes the second-order dispersion (β_2) curves of the fundamental core mode along with the different waveguide widths. We employ the single span of exponentially GVD decreasing tapered silicon waveguide with a serious of straight waveguide segments of constant dispersions, which is a stepwise approximation method. We numerically explore the influence of dividing the tapered silicon wavguide into 8, 16 and 32 parts where the error of the output pluse width between 16 parts and 32 parts is less than 5%, hence we divide the waveguide into 16 parts in the following discussion. In Fig. 2(a), the β_2 lines are monotonically decreasing at the

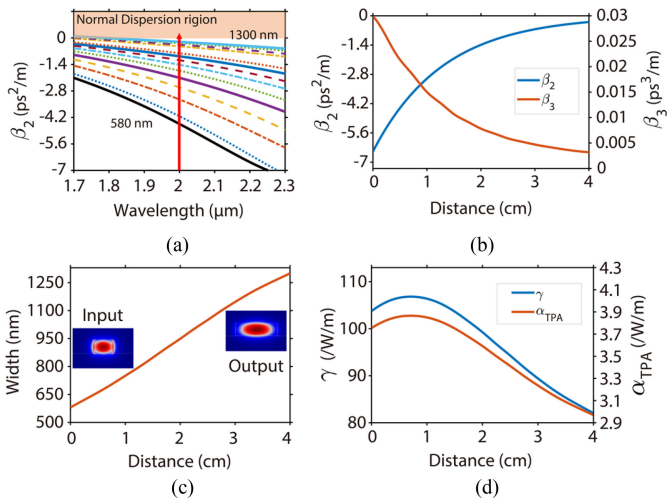

Fig. 2. Dispersion and nonlinearity parameters of the tapered silicon waveguide. (a) Second-order dispersion (β_2) of the fundamental core mode for various waveguide widths from 580 to 1300 nm. The red vertical line presents the wavelength of 2000 nm. (b) Calculated β_2 and third-order dispersion (β_3) along with propagating distance. (c) Waveguide width as a function of propagation distance. The insert electric-field distribution denotes the mode patterns of the input and output waveguide taper interfaces. (d) Nonlinear coefficient (γ) and TPA loss coefficient (α_{TPA}) curves along with propagation distance.

wavelength from 1.7 μm to 2.3 μm. Besides, the value of β_2 at the center wavelength of 2.0 μm declines along with the waveguide widths from 580 nm to 1300 nm, which is indicated by the red vertical line in Fig. 2(a). Fig. 2(b) represents the computed β_2 and third-order dispersion (β_3) for tuned propagation distance, which are calculated by finite element method. The proposed waveguide is characterized by GVD decreasing exponentially from -6.49 ps^2/m to -0.30 ps^2/m and β_3 reduces from 0.030 ps^3/m to 0.003 ps^3/m. As shown in Fig. 2(c), the waveguide width from 580 nm to 1300 nm is close to linearly increasing along with the tapered silicon waveguide. With the development of the waveguide fabrication technicque [34], [35], the proposed silicon-based waveguide can be manufactured with a high-precision CMOS facility. Fig. 2(d) plots the nonlinearity and TPA loss performance, where γ reduces from 103.72 /W/m to 82.03 /W/m and α_{TPA} declines from 3.75 /W/m to 2.97 /W/m. Modal distribution integrals $\int\int_{-\infty}^{+\infty} |F(x,y)|^2 dxdy$ and $\int\int_{-\infty}^{+\infty} |F(x,y)|^4 dxdy$ increase monotonically along with the waveguide widths from 580 nm to 1300 nm, while the variation of γ and α_{TPA} are not monotonic since the effective mode area is associated with $\left(\int\int_{-\infty}^{+\infty} |F(x,y)|^2 dxdy\right)^2$ and $\int\int_{-\infty}^{+\infty} |F(x,y)|^4 dxdy$ in the Eqs. (3) and (4).

B. Numerical Results of Two Pulses Combination and Compression With the Same Center wavelengths.

It is interesting to understand the formation dynamics of Si-TPCC, and we utilize two RC pulses as the input signal to investigate the pulse dynamics, where we consider $\Delta\nu = 0$ as both the pulses are chosen to be of the same wavelengths and the other pulse parameters are $\alpha_{20} = -11.89\ \mathrm{THz}^2$, $P_0 = 1.08\,\mathrm{W}$ and $T_0 = 274.8\,\mathrm{fs}$ which refers that the full width at half-maximum

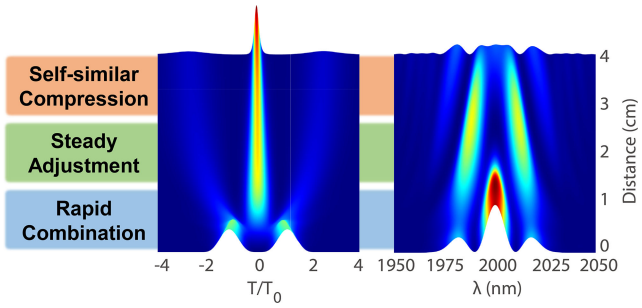

Fig. 3. Sketch of the temporal and spectral evolution for the two pulses combination and compression buildup process, including rapid combination, steady adjustment and self-similar pulse compression.

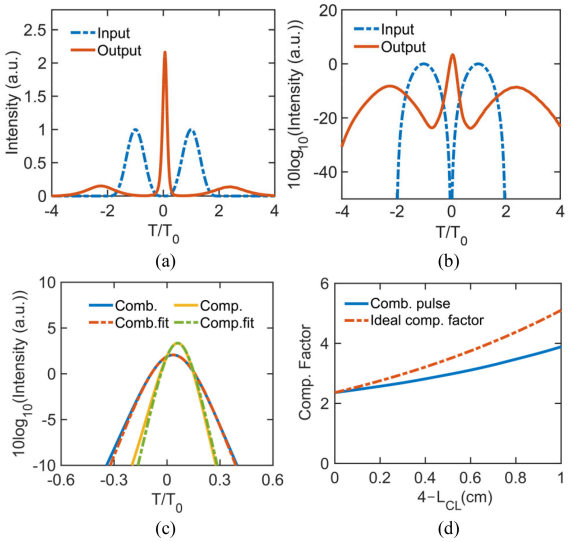

Fig. 4. Numerical simulations of two pulses combination and compression with the same center wavelengths of 2000 nm. The two input RC pulses and output compressed pulse profiles in (a) linear scales and (b) logarithmic scales. (c) The combined pulse and compressed pulse compared with their fitted hyperbolic secant pulses in logarithmic scales. (d) The compression factor curves of the simulation and the ideal compression factor during the final 1 cm waveguide.

(FWHM) of two input pulses are both 200 fs. Since silicon waveguide has a huge Kerr nonlinearity and governed by small TPA loss mechanisms at 2.0 μm [4], the comparatively small initial peak powers are necessary for the initiate compression. In Fig. 3, the input pulses undergo a serial of particular stages containing rapid combination, steady adjustment and self-similar pulse compression. In the rapid combination, the temporal intensity of the input pulses noticeably declines after propagating 1 cm and the single center pulse is initially formed with the FWHM of 151 fs. Then, the new single pulse further evolves into a combined pulse during the steady adjustment process; meanwhile, the original pulses transform into the pedestal. Here, the combination length (L_{CL}) is presented as the waveguide distance that the peak power of the pedestal is lower than 10% of the main peak for the combined pulse, and the combination length is 3 cm. Consequently, the combined pulse is successfully observed to realize efficient self-similar pulse compression in advanced on-chip device.

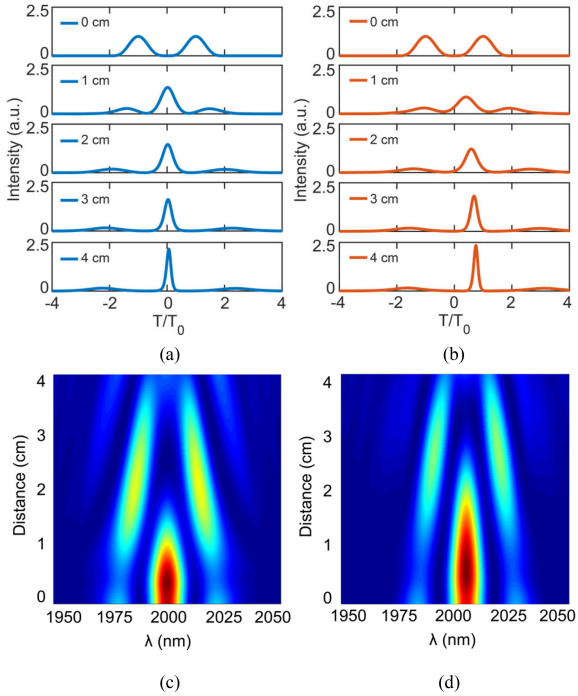

Fig. 5. Temporal evolutions of two RC pulses along the tapered silicon waveguide for (a) the same center wavelength of 2000 nm and (b) different central wavelengths of $\lambda_0 = 2000\,\text{nm}$ and $\lambda_1 = 2010\,\text{nm}$. Contour plot of normalized spectrum distributions for the two pulses combination and compression buildup process with the (c) same and (d) different central wavelengths.

As shown in Fig. 4(a) and (b), the pulse duration is reduced to 49.0 fs which possesses the compression factor of 4.08 for the final output pulse. In addition, the peak power of the single pulse increases to 2.16 times of the initial peak power, which is corresponding to the peak power ratio of 2.16. Si-TPCC demonstrates a unique superiority that the time bandwidth product (TBP) of the compressed pulse is 0.33, which remains the transform-limited hyperbolic secant pulse. Fig. 4(c) represents that the combined pulse and compressed pulse compared both are almost retaining the hyperbolic secant pulses. The combination length was found to be 3 cm in which the pulse width decreased to 82 fs. During the buildup process, the initial linear chirp promotes the interaction between decreasing dispersion and self-phase modulation effects. In Fig. 4(d), the two compression factor curves share the comparable trend in the final 1 cm waveguide, which reveals that the compression factor of the compressed pulse is 4.08 and the ideal compression factor value of 5.4 is calculated from self-similar pulse compression analytical expression [24].

C. Numerical Results of Two Pulses Combination and Compression With the Different Center Wavelengths

We then explore two pulses combination and compression based on different laser sources to perceive the formation dynamics associated with the different center wavelengths. Fig. 5 reveals a representative simulation of Si-TPCC for the same center wavelength of 2000 nm and the different center wavelengths of 2000 nm and 2010 nm, which employs the temporal evolution and spectral intensity contour plot. Thanks to the contribution

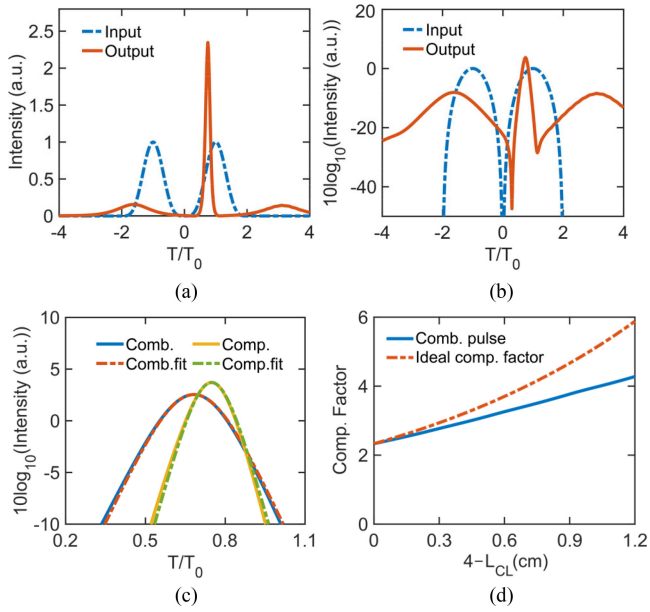

Fig. 6. Numerical simulations of two pulses combination and compression for different center wavelengths of $\lambda_0 = 2000\,\mathrm{nm}$ and $\lambda_1 = 2010\,\mathrm{nm}$. The two input RC pulses and output compressed pulse profiles in (a) linear scales and (b) logarithmic scales. (c) The combined pulse and compressed pulse compared with their fitted hyperbolic secant pulses in logarithmic scales. (d) The compression factor curves of the simulation and the ideal compression factor during the final 1.2 cm waveguide.

of the shared initial chirp, two pulses transfer towards the zero point of the time coordinate axis firstly and then coalesce into a new single pulse at the combintion length around 3 cm in Fig. 5(a). In the remaining propagation distance, the combined pulse achieves nearly self-similar compressed and transformed into a soliton-like pulse. Fig. 5(b) reveals two pulses combination and compression with different center wavelengths, which represents a similar trend to Fig. 5(a). Note that the compressed pulse with different central wavelength experences obvious temporal shift than that of the same central wavelength in Fig. 5(a). Fig. 5(c) and (d) illustrate the normalized spectrum distributions of the Si-TPCC. We observe that the spectrum remains perfect symmetry under the influence of strong SPM effect and the intensity of the spectrum shifts to both sides.

In order to demonstrate the Si-TPCC characterization with the different center wavelengths of 2000 nm and 2010 nm, we consider $\Delta\nu = 0.746$ as the variation between the center frequencies of the two input pulses and the other pulse parameters remain the same value. As shown in Fig. 6(a) and (b), we observe the temporal profile of the input and output pulses in (a) linear and (b) logarithmic scales, where the initial pulse width can be compressed from 200 fs to 46.0 fs with the compression factor of 4.35 and the peak power ratio of 2.35. Note that the compressed pulse poccesses the advantages that the TBP reaches 0.38, which maintains the transform-limited hyperbolic secant pulse. Fig. 6(c) reveals that the input pulses firstly merge into a single pulse at the combination length of 2.8 cm with the combined pulse width of 83.83 fs. Additionally, the combined pulse and compressed pulse fit perfectly with the

TABLE I
COMPRESSION FACTOR, TBP, PEAK POWER RATIO AND COMBINATION LENGTH FOR SI-TPCC WITH THE SAME AND DIFFERENT CENTER WAVELENGTHS

	$\lambda_0 = \lambda_1 = 2000$ nm	$\lambda_0 = 2000$ nm, $\lambda_1 = 2010$ nm
Compression Factor	4.08	4.35
TBP	0.33	0.375
Peak Power Ratio	2.16	2.35
Combination Length (cm)	3	2.8

hyperbolic secant pulses. In the Fig. 6(d), the combined pulse realize nearly self-similar pulse compression in the final 1.2 cm waveguide, which is similar to Fig. 4(d). The compression factor of the output pulse is 4.35 and the ideal compression factor value of 6.06 is considered from self-similar pulse compression analytical expression [24]. The corresponding results of the same and different center wavelengths are denoted in the Table I. As it takes a comparable perfomance of the compressed pulse, we further demonstrate that the Si-TPCC scheme works effciently with the different light sources. This results indicates that two input pulses from different center wavelengths can realize high-degree combination and compression by suitably chirping pulses and propagating in the exponentially dispersion decreasing silicon waveguide.

D. Numerical Results of Two Pulses Combination and Compression With the Different Center Wavelengths

Another important investigation is to explore the influence of the separation between the center wavelengths for the two pulses combination and compression. Hence, we illustrate the simulation results by fixing one of input pulse center wavelength ($\lambda_0 = 2000\,\mathrm{nm}$) and altering the other input pulse center wavelength (λ_1) from 1990 nm to 2010 nm, where the corresponding $\Delta\nu$ is from -0.75 THz to 0.75 THz. Furthermore, the input single pulse bandwidth (λ_{FWHM}) is calcaulated as 35.43 nm in the Eqs. (8) or (9), indicating that the wavelength separation ratio (WSR, $(\lambda_1 - \lambda_0)/\lambda_{\mathrm{FWHM}}$) change from -0.28 to 0.28. In Fig. 7(a), as we expands WSR from -0.28 to 0.28, the center of the main lobe moves monotonically forward from -0.64 to 0.75 in the normalized temporal field, while the coresponding normalized intensity enhancing firstly from 1.44 to 2.34. Fig. 7(b1)–(b3) further plot the pulse propagation dynamics with the different WSR of -0.28, 0 and 0.28. In Fig. 7(b1), the combined pulse is a higher-order soliton due to the WSR shift for -0.28, where the combined pulse is accompanied by breathing effect and the output pulse width increasing to 165 fs. As shown in Fig. 7(b2), the initial peak power is sufficient to match combination pulse as the fundamental pulse condition for WSR=0 that the input pulses achieve perfect combination at 3 cm and then realizes optimum self-similar pulse compression to 49.0 fs. Fig. 7(b3) presents the pulse combination and compression process as WSR $= 0.28$, where the corresponding combintion length is 2.8 cm and output pulse width is 46.0 fs. Note that the initial

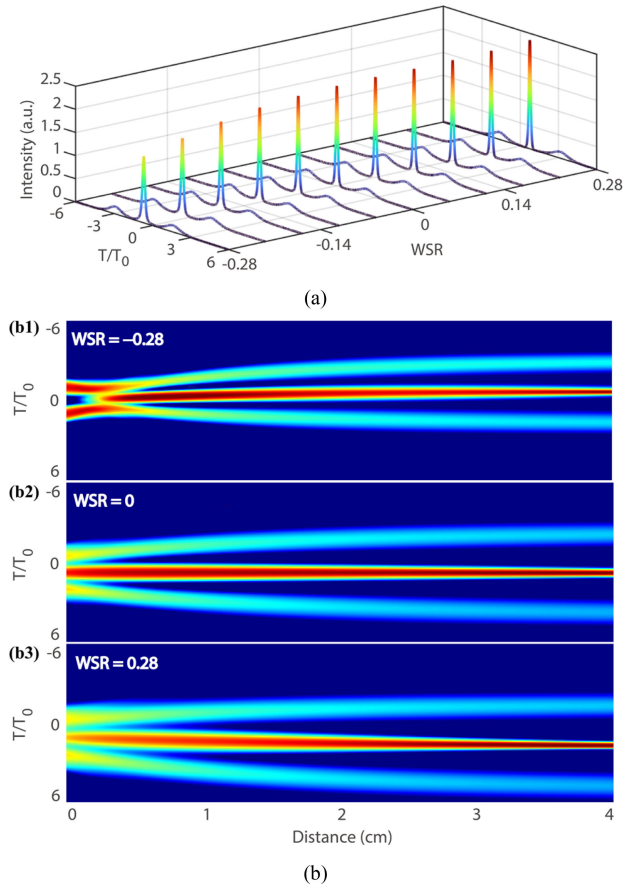

Fig. 7. Combination and compression formation dynamics of two input pulses for different WSR. (a) Output compressed pulse profiles. (b1)-(b3) side view of two pulses propagation with different WSR of −0.28, 0 and 0.28, respectively.

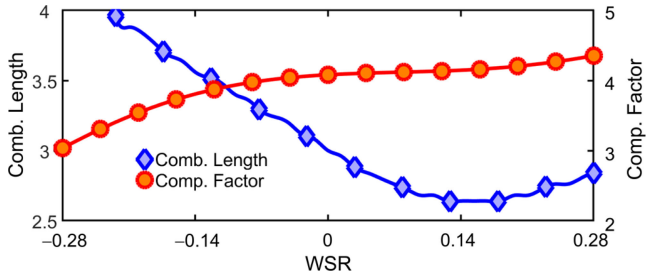

Fig. 8. The dependences of combination length and compression factor versus separated WSR of output pulse.

center wavelength shift causes the pulse center has slightly offset in Fig. 7(b1) and (b3).

Si-TPCC can provide a flexible adjustment range for separated center wavelengths to generate a high-performance compressed pulse. The evolutions of combination length and compression factor during WSR from −0.28 to 0.28 are deciped in Fig. 8, where T_0 and α_{20} remain the same values as Fig. 2. The input pulses preserve self-adjusts and combination due to the balance between dispersion and nonlinearity simultaneously. Therefore, the different center wavelengths shift exhibit similar performance as the same center wavelengths. The combination length curve is represented a downward trend, which indicates that L_{CL} reaches up to the minimum value of 2.64 cm at WSR = 0.14. Furthermore, the compression factor curve express as monotonically increasing and the maximum compression factor can be acquired as 4.35 at WSR = 0.28.

IV. Conclusion

In conclusion, we report the two RC pulses simultaneous combination and effective compression in the exponentially decreasing dispersion silicon waveguide, which is based on the precisely engineered dispersion. As we consider the same initial center wavelengths of 2000 nm, two initial RC pulses can realize a compression factor of 4.08 and the peak power ratio of 2.16. Furthermore, even as we employ the different center wavelengths of 2000 nm and 2010 nm, the Si-TPCC scheme is also valid that the compression factor attains 4.35 and the final peak power ratio reach up to 2.35. During the buildup process, the input pulses go through rapid combination, steady adjustment and self-similar pulse compression stages. Moreover, we examine the influence of the initial center wavelength separation by fixing one of input pulse center wavelength of 2000 nm and altering the other input pulse center wavelength from 1990 nm to 2010 nm, which reveals that two input pulses can successfully realize combination and compression. Our findings supply the guidelines to fully control the rich dynamics of more input pulses numbers (e.g., 3, 4, 5 and N input pulses) to realize pulses combination and self-similar compression in the integrated devices, key for future deployment of mid-infrared high brightness spectroscopy in the molecular fingerprint region.

References

[1] A. H. Jones, S. D. March, S. R. Bank, and J. C. Campbell, "Low-noise high-temperature AlInAsSb/GaSb avalanche photodiodes for 2-μm applications," *Nature Photon.*, vol. 14, no. 9, pp. 559–563, 2020.

[2] N. M. Fried and P. B. Irby, "Advances in laser technology and fibre-optic delivery systems in lithotripsy," *Nature Rev. Urol.*, vol. 15, no. 9, pp. 563–573, 2018.

[3] W. Lai *et al.*, "Sub-200 fs, 344 MHz mode-locked Tm-doped fiber laser," *Opt. Lett.*, vol. 45, no. 19, pp. 5492–5495, 2020.

[4] B. Kuyken *et al.*, "An octave-spanning mid-infrared frequency comb generated in a silicon nanophotonic wire waveguide," *Nature Commun.*, vol. 6, no. 1, 2015, Art. no. 6310.

[5] J. Ma, Z. Qin, G. Xie, L. Qian, and D. Tang, "Review of mid-infrared mode-locked laser sources in the 2.0 μm–3.5 μm spectral region," *Appl. Phys. Rev.*, vol. 6, no. 2, 2019, Art. no. 021317.

[6] J. Wang *et al.*, "Generation of few-cycle pulses from a mode-locked Tm-doped fiber laser," *Opt. Lett.*, vol. 46, no. 10, 2021, Art. no. 2445.

[7] C. Gaida *et al.*, "Watt-scale super-octave mid-infrared intrapulse difference frequency generation," *Light Sci. Appl.*, vol. 7, no. 1, 2018, Art. no. 94.

[8] A. Schliesser, N. Picqué, and T. W. Hänsch, "Mid-infrared frequency combs," *Nature Photon.*, vol. 6, no. 7, pp. 440–449, 2012.

[9] J. W. Choi *et al.*, "High spectro-temporal compression on a nonlinear CMOS-chip," *Light Sci. Appl.*, vol. 10, no. 1, 2021, Art. no. 130.

[10] P. Colman, C. Husko, S. Combrié, I. Sagnes, C. W. Wong, and A. De Rossi, "Temporal solitons and pulse compression in photonic crystal waveguides," *Nature Photon.*, vol. 4, no. 12, pp. 862–868, 2010.

[11] A. Blanco-Redondo *et al.*, "Observation of soliton compression in silicon photonic crystals," *Nature Commun.*, vol. 5, no. 1, 2014, Art. no. 3160.

[12] J. W. Choi, B. U. Sohn, G. F. R. Chen, D. K. T. Ng, and D. T. H. Tan, "Soliton-effect optical pulse compression in CMOS-compatible ultra-silicon-rich nitride waveguides," *APL Photon.*, vol. 4, no. 11, 2019, Art. no. 110804.

[13] E. Sahin *et al.*, "Bragg soliton compression and fission on CMOS-compatible ultra-silicon-rich nitride," *Laser Photon. Rev.*, vol. 13, no. 8, 2019, Art. no. 1900114.
[14] S. Lavdas, J. B. Driscoll, R. R. Grote, R. M. Osgood, and N. C. Panoiu, "Pulse compression in adiabatically tapered silicon photonic wires," *Opt. Exp.*, vol. 22, no. 6, pp. 6296–6312, 2014.
[15] C. Mei *et al.*, "Self-similar propagation and compression of the parabolic pulse in silicon waveguide," *J. Lightw. Technol.*, vol. 37, no. 9, pp. 1990–1999, May 2019.
[16] J. Huang, F. Ye, and Q. Li, "Mid-infrared cascaded soliton compression on CMOS-compatible silicon waveguide," *J. Lightw. Technol.*, vol. 40, no. 4, pp. 1098–1104, Feb. 2022.
[17] J. Yuan *et al.*, "Mid-infrared self-similar compression of picosecond pulse in an inversely tapered silicon ridge waveguide," *Opt. Exp.*, vol. 25, no. 26, pp. 33439–33450, 2017.
[18] J. Huang, M. S. A. Gandhi, and Q. Li, "Self-similar chirped pulse compression in the tapered silicon ridge slot waveguide," *IEEE J. Sel. Topics Quantum Electron.*, vol. 26, no. 2, Mar./Apr. 2020, Art. no. 8300508.
[19] C. Mei *et al.*, "High degree picosecond pulse compression in chalcogenide-silicon slot waveguide taper," *J. Lightw. Technol.*, vol. 34, no. 16, pp. 3843–3852, Aug. 2016.
[20] F. Ye, J. Huang, M. S. A. Gandhi, and Q. Li, "Nearly self-similar pulse compression of high-repetition-rate pulse trains in tapered silicon waveguides," *J. Lightw. Technol.*, vol. 39, no. 14, pp. 4717–4724, Jul. 2021.
[21] Y. Cheng *et al.*, "Self-similar picosecond pulse compression for supercontinuum generation at mid-infrared wavelength in silicon strip waveguides," *Opt. Commun.*, vol. 454, 2020, Art. no. 124380.
[22] D. R. Carlson, P. Hutchison, D. D. Hickstein, and S. B. Papp, "Generating few-cycle pulses with integrated nonlinear photonics," *Opt. Exp.*, vol. 27, no. 26, 2019, Art. no. 37374.
[23] J. D. Moores, "Nonlinear compression of chirped solitary waves with and without phase modulation," *Opt. Lett.*, vol. 21, no. 8, pp. 555–557, 1996.
[24] Q. Li, Z. Jian, W. Lu, K. Nakkeeran, K. Senthilnathan, and P. K. A. Wai, "Combination and compression of multiple optical pulses in nonlinear fibers with the exponentially decreasing dispersion," *IEEE J. Quantum Electron.*, vol. 54, no. 2, Apr. 2018, Art. no. 6800110.
[25] J. Huang, Q. Li, Z. Jian, P. K. A. Wai, and K. Nakkeeran, "Combination and compression of multiple pulses with same or different wavelengths," *J. Lightw. Technol.*, vol. 38, no. 24, pp. 6932–6938, Dec. 2020.
[26] W. Shen *et al.*, "Chalcogenide glass photonic integration for improved 2 μm optical interconnection," *Photon. Res.*, vol. 8, no. 9, 2020, Art. no. 1484.
[27] X. Wang *et al.*, "High-speed silicon photonic Mach–Zehnder modulator at 2 μm," *Photon. Res.,* vol. 9, no. 4, pp. 535–540, 2021.
[28] F. Leo *et al.*, "Dispersive wave emission and supercontinuum generation in a silicon wire waveguide pumped around the 1550 nm telecommunication wavelength," *Opt. Lett.*, vol. 39, no. 12, pp. 3623–3626, 2014.
[29] H. Saghaei and V. Van, "Broadband mid-infrared supercontinuum generation in dispersion-engineered silicon-on-insulator waveguide," *J. Opt. Soc. Amer. B*, vol. 36, no. 2, pp. A193–A202, 2019.
[30] L. Yin and G. P. Agrawal, "Impact of two-photon absorption on self-phase modulation in silicon waveguides," *Opt. Lett.*, vol. 32, no. 14, pp. 2031–2033, 2007.
[31] X. Gai *et al.*, "Nonlinear absorption and refraction in crystalline silicon in the mid-infrared," *Laser Photon. Rev.*, vol. 7, no. 6, pp. 1054–1064, 2013.
[32] L. Yin, Q. Lin, and G. P. Agrawal, "Soliton fission and supercontinuum generation in silicon waveguides," *Opt. Lett.*, vol. 32, no. 4, pp. 391–393, 2007.
[33] A. D. Bristow, N. Rotenberg, and H. M. van Driel, "Two-photon absorption and Kerr coefficients of silicon for 850–2200 nm," *Appl. Phys. Lett.*, vol. 90, no. 19, 2007, Art. no. 191104.
[34] N. Singh *et al.*, "Octave-spanning coherent supercontinuum generation in silicon on insulator from 1.06 μm to beyond 2.4 μm," *Light Sci. Appl.*, vol. 7, no. 1, pp. 17131–17131, 2018.
[35] N. Singh *et al.*, "Midinfrared supercontinuum generation from 2 to 6 μm in a silicon nanowire," *Optica*, vol. 2, no. 9, pp. 797–802, 2015.